Supplementary Information: The influence of off-fault deformation zones on the near-fault distribution of coseismic landslides

Table of Contents

ADDITIONAL METHODOLOGY

Here we present supplementary information and figures (Fig. DR1 and DR2) to demonstrate the methodology of the ICP analysis. Displacement profiles were taken perpendicular to local fault strike and OFD was estimated in these profiles (DR2). In some cases, our defined OFD zone includes the effect of slip on multiple fault strands.
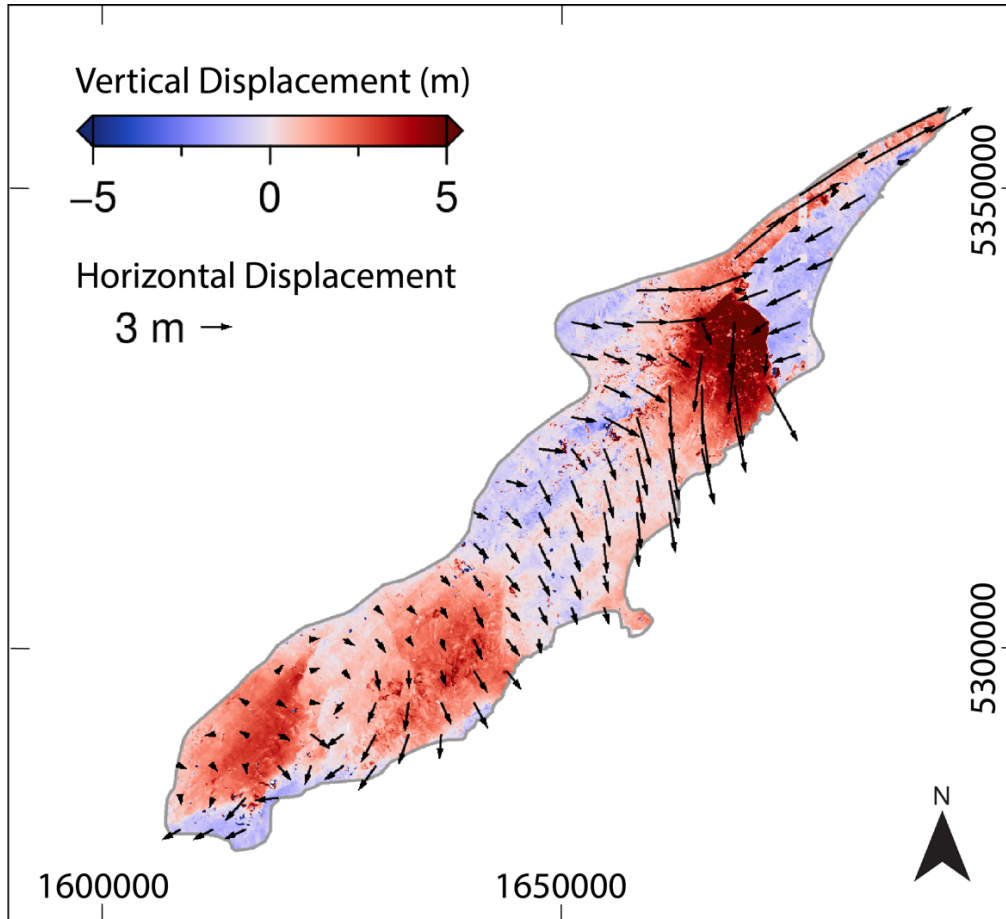

Figure DR1. Three-Dimensional displacement fields for the 2016 Kaikōura earthquake, generated from pre- and post-event aerial imagery using the iterative closest point technique. The colormap shows vertical displacements while the vectors represent median horizontal displacements over 5 km-wide areas (downsampled from the 25 m we used for analyses) centered on each arrow. Coordinates are in meters in the New Zealand Transverse Mercator projection.
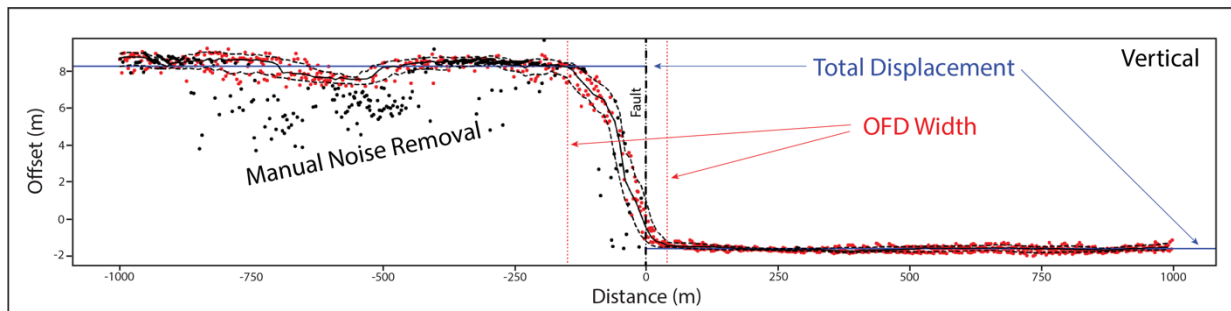

Figure DR2. An example vertical displacement profile across the Papatea Fault (Figure 1). Black data points represent identifiable noise that was manually removed from the profile. OFD width (red vertical lines) on either side of the fault (black vertical line) are manually placed where the profile rollover reaches the background displacement.

As stated in the main text, we generated separate displacement profiles in each of the east, north, and vertical directions. This allowed us to remove noise from identifiable sources (e.g. landslides, fast-growing trees) from each displacement direction separately and improved our ability to interpret the tectonic signal and width of OFD in the profiles.

ADDITIONAL ANALYSIS AND OUTCOMES

We conducted the following analyses in addition to those described in the text.

Distance from Fault 'Hypocenter'

Previous studies have demonstrated a relationship between landslide density and distance from earthquake hypocenter (e.g., Meunier et al., 2007). Determining landslide attenuation with distance from the hypocenter is quite complicated in the case of the multi-fault Kaikōura earthquake where the true hypocenter lies over 100 km south of some of the largest fault ruptures (Fig. DR3). To best approximate attenuation for the Kaikōura event, we calculated 3-D distance to the nearest point of initiation on modeled fault planes from two separate modeling efforts by Bradley et al., (2017) and Holden et al. (2017), referred to herein as the Bradley and Holden hypocenters (Fig. DR3).
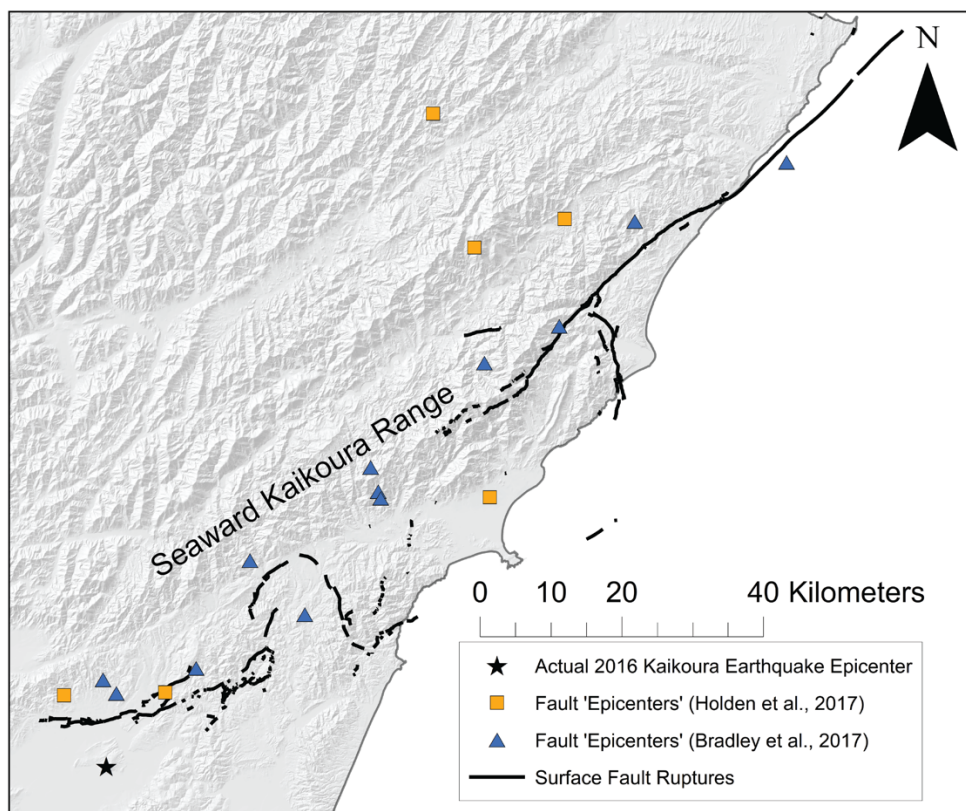

Figure DR3. Map showing the location of individual fault 'epicenters' derived from modeling by Holden et al. (2007) and Bradley et al. (2007).

Using 'distance to the hypocenter' we followed similar methods to the main text to determine landslide density trends using gridded landslide data from Massey et al. (2020). We produced 200 equally spaced bins for the two datasets and excluded landslide density derived from less than 0.1% of the total gridded area (a min. of c. 3500 grid cells) to limit bias in the landslide density trend.

Despite different 'hypocenters' the two modeling efforts resulted in similar, arguably non-linear, landslide density trends that decrease with distance from the hypocenter across the Kaikōura region (Fig. DR4A). Interestingly, both landslide density trends drop sharply close to the hypocenter where the greatest landslide density would be expected. To determine the robustness of the 'distance to hypocenter' parameter in the case of the 2016 Kaikoura earthquake, we investigated how the distance from hypocenter trends compared to other predictive factors including lithology and topography (Fig. DR4B-D).
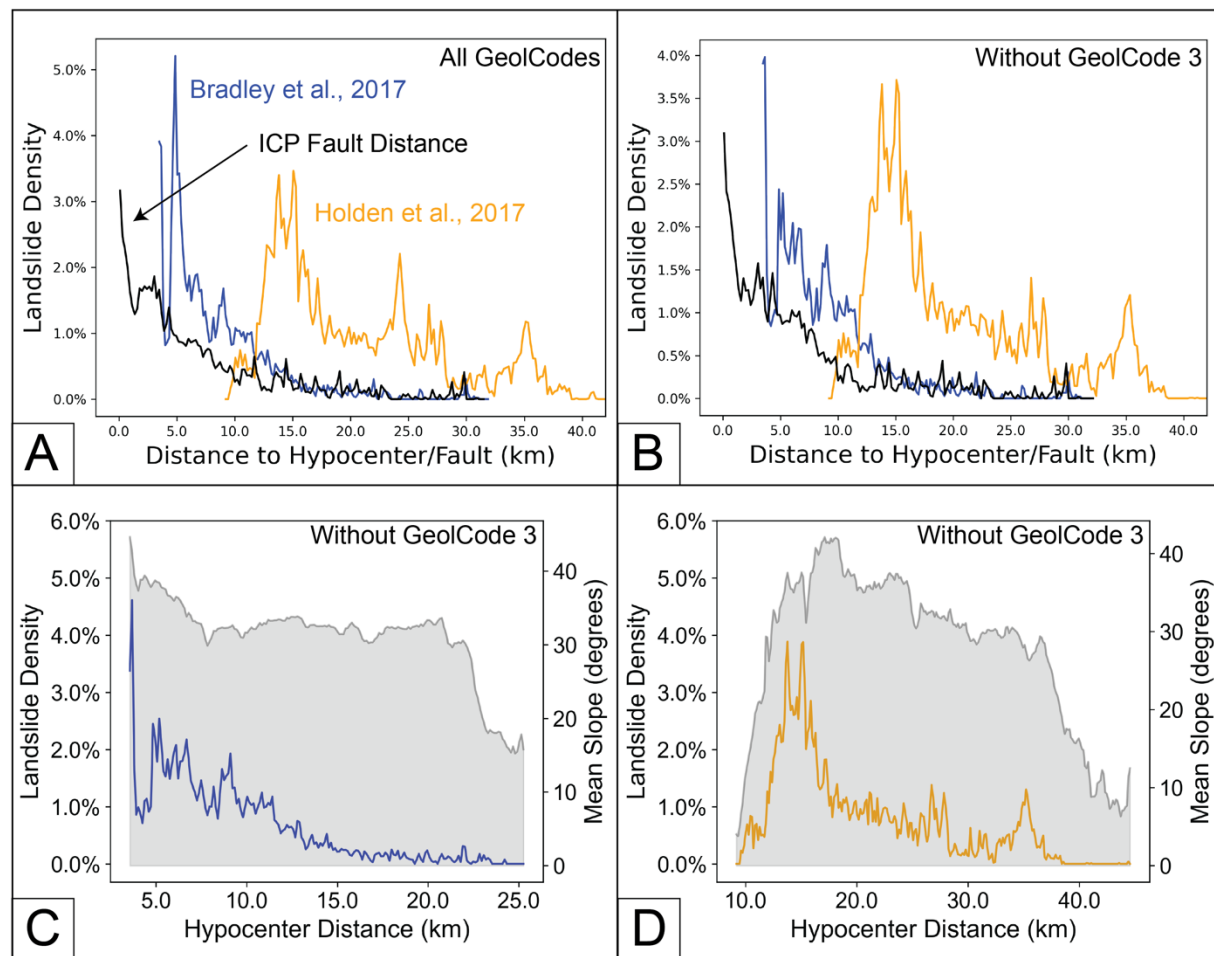

Figure DR4. Graphs of Landslide density to Distance from the Hypocenter/Distance from Fault. Distance to 'Hypocenter' is defined by 3-D distance to the nearest point of initiation on modeled fault planes by Bradley et al. (2017) (Blue Line) and Holden et al. (2017) (Orange Line) and distance to fault as distance to ICP derived surface fault ruptures (Black Line). Landslide density in (A) all Geology types (GeolCode) and (B-D) all Geology types except GeolCode3 (Upper Cretaceous to Paleogene Sedimentary Rocks and Minor Volcanics). Landslide density compared to mean slope (grey) for (C) Bradley hypocenters and (D) Holden hypocenters.

Our best explanations for the observed landslide density trends are as follows: (1) The Bradley hypocenters capture a large spike in landslide density around 5 km (Fig. DR4A). This occurs due to a coincidental spike in landslide density within GeolCode 3 (*Upper Cretaceous to Paleogene Sedimentary Rocks and Minor Volcanics)* that does not appear to significantly influence the other two landslide density trends (Fig. DR4B). (2) Both the Bradley and Holden hypocenters correlate strongly with topographic influences including slope, particularly at smaller distances from the hypocenter (Fig. DR4C-D). As an example, after removing GeolCode 3, the remaining large peak in landslide density with distance from the Bradley hypocenters matches closely with a c. 5° spike in mean slope (Fig. DR4C). (3) In both cases, hypocentral distance appears to capture the general attenuation of ground motion with distance from the source but neither fully accounts for the complicated ground motion interactions introduced by rupture on more than 20 faults.

We believe that more robustly defined modeled PGA by Bradley et al. (2017), as opposed to 'distance from the hypocenter', remains the better point of comparison with the distance from fault trends. Although modeled PGA is relatively linear near the fault (Fig. 3A in main text) and matches with sparse strong ground motion observations, it remains possible that real ground motions attenuate non-linearly from the fault. If this is the case, the observed 'distance to fault' landslide density trend may be more correlated to ground motion attenuation than modeled PGA would lead us to believe. Regardless, we do not believe that this uncertainty about near-fault ground motions changes our final conclusions about the OFD zone. If the surface fault rupture had no influence on landslide density and, instead landslide density was entirely defined by the attenuation of ground motion from the source, we would not expect to observe a higher landslide density within the OFD zone as compared to general distance from the fault (Fig 3A in main text). It remains likely that, even if ground motion attenuation is non-linear, factors associated with fault damage contribute significantly to landslide density within the OFD zone.

There is additional evidence that the distribution of landslides we observe with distance from the fault is not an exclusive product of hypocentral distance or geometric spreading as described by Meunier et al (2007). For the 'distance from fault' landslide density trend we observe to correlate to hypocentral distance, fault ruptures would need to occur on faults with near vertical dip and/or with extremely shallow source depths (Fig. DR5). This is unlikely for two reasons: (1) Fault dips in the Kaikōura region are often steep (c. $69 \pm 13°$; Litchfield et al., 2018) but are rarely vertical. (2) Source depths would need to be implausibly shallow (c. < 1 km depth) on dipping faults to produce a similar trend. If landslide density from the Kaikōura earthquake was primarily the result of geometric spreading away from the ground motion source, rather than the observed attenuation, we would expect to observe a somewhat normal distribution of landslide density centered away from the surface fault ruptures as previously demonstrated for other events by Meunier et al. (2007; Fig. DR5).
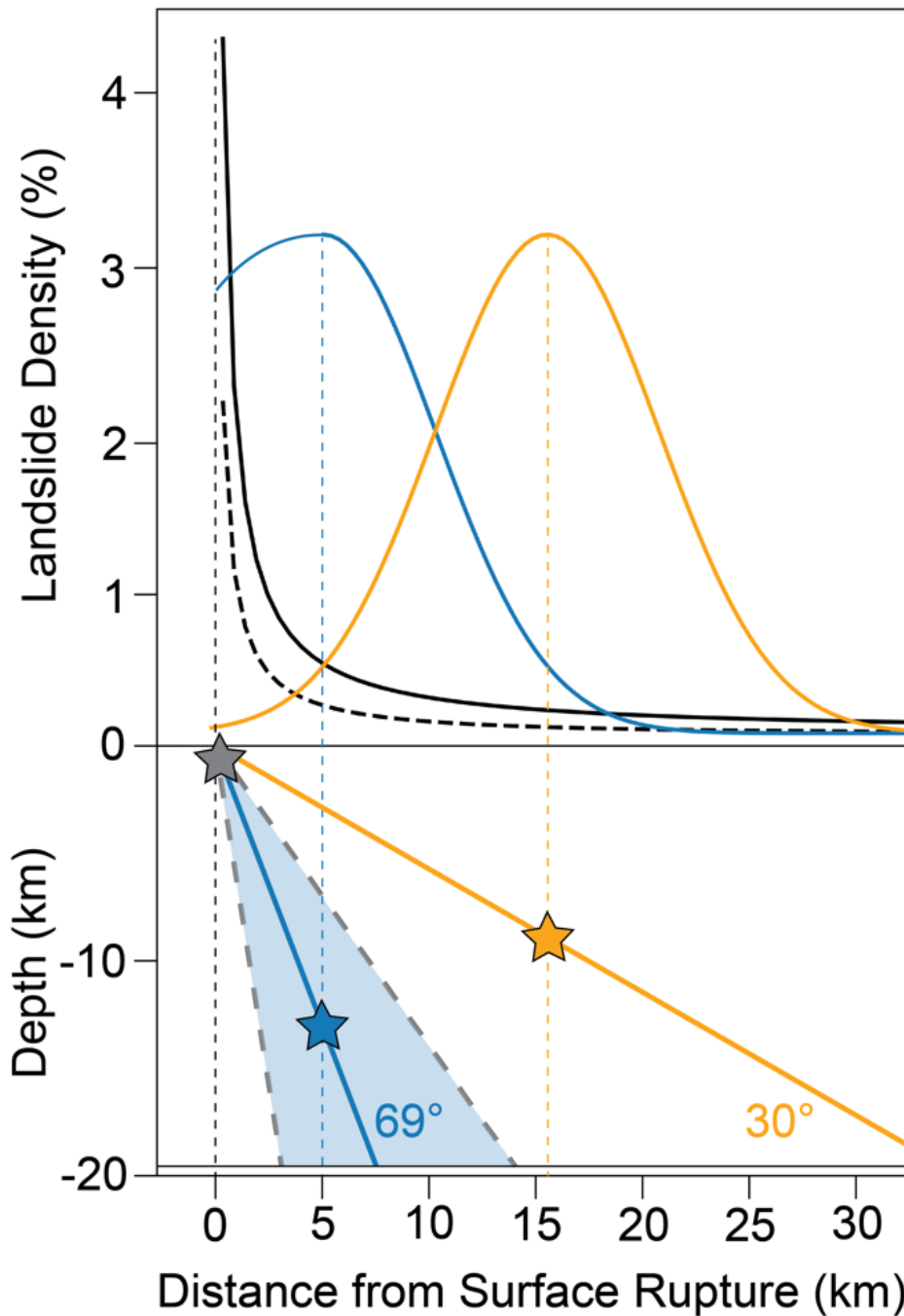
Figure DR5. Schematic representation of landslide density (percentage of total area) plotted with distance to surface fault rupture. Hypothetical fault planes and dips are shown in blue and orange along with the position of hypothetical earthquake hypocenters (stars). The solid black line represents a similar distribution to the observed landslide density from the 2016 Kaikōura earthquake. Assuming hypocentral distance, as a product of geometric spreading, is the primary influence on landslide density, with distance from the fault, peaks in landslide density should be located immediately above the earthquake hypocenter. To achieve the observed landslide density distribution with distance from the hypocenter, dips would need to be near vertical and/or have an extremely shallow source depth. Major faults that ruptured during the Kaikōura earthquake have dips c. 69 ± 13° (Blue shaded region, Litchfield et al., 2018). Applying a damping factor (e.g. Meunier et al., 2007) modulates the landslide density distribution; for example, applying a damping factor to a vertical dip scenario results in the dashed black landslide density curve.

Topographic Influence on the OFD Zone

To determine the influence of topography on landslide density within the OFD zone, we compared the density of slopes within the OFD zone to the density of slopes within 1000 m of surface fault ruptures as defined in our analysis (Fig. DR6). We observed a generally similar distribution of slope with some limited topographic sampling bias where the OFD zone sampled a smaller proportion of low slopes (less than 10°).

To ensure that the distribution of landslides within the OFD zone was not simply a reflection of the above-mentioned sampling bias, we conducted the same landslide density analysis using the 30x30 m binary landslide source area grid by Massey et al. (2020) where slope values were greater than 10°. The 10° slope threshold captures ~ 98.5% of the landslide source area across the Kaikōura region while eliminating most flat areas. The comparative landslide densities showed nominally higher but relatively consistent landslide densities for the OFD zone (Fig. DR6). Interestingly, when we removed slopes less than 10°, despite seeing little change in the trend of landslide density, we did observe a slightly greater proportion of lower slope angles (c. 20-40°) represented within the OFD zone as compared to the area within 1000 m of the fault.
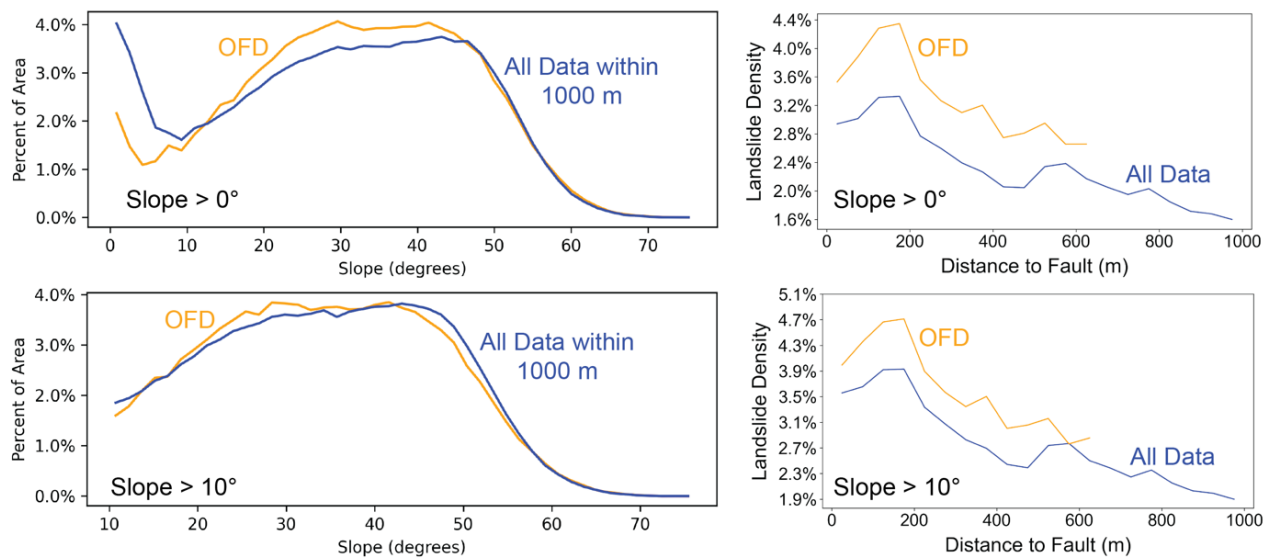

Figure DR6. Graphs comparing density of Slope within the OFD zone to the density of slope within 1000 m of surface fault ruptures (Right) and landslide density within the OFD Zone as compared to general distance to surface fault ruptures (Left). When conducting our analysis on slopes greater than 10 degrees, to account for the influence of topography on the distribution of landslide within the OFD zone, we observe a similar trend in landslide density despite an increased proportion of lower slopes within the OFD zone as compared to the general area within 1000 m of the fault.

Local Slope Relief

Local Slope Relief (LSR) shows a very similar trend to Slope (as shown in Fig. 3C) with a lower LSR near the fault increasing with distance from the fault (Fig. DR7.)
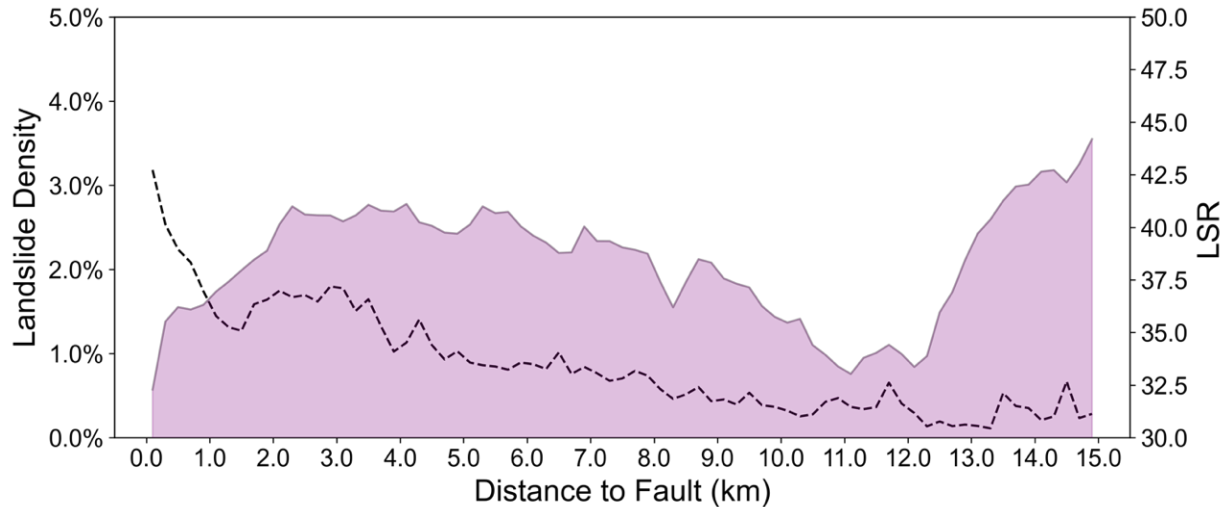
Figure DR7. Landslide Density and Local Slope Relief (LSR) to Fault Distance graph. Landslide density in 200 m bins (Dashed Black Line) decreases with distance from the fault while LSR (purple area) increases with distance from the fault to c. 2000 m from the fault.

Geology and OFD

Lithology in combination with topography, strong ground motion, and near fault processes has a strong influence on the distribution of landslides with distance from the fault (e.g. Meunier et al., 2013; Massey et al., 2020; Rault et al., 2019). As an example, we observe different trends in landslide density between Torlesse and non-Torlesse lithology with distance from the fault (Figure 3D). This variability is largely a product of different lithologic responses to slope, strong ground motion, and near-fault factors.

To ensure that this variability in lithology did not also contribute to our finding of a higher landslide density in the OFD zone, we conducted the following analyses:

> 1. We examined the landslide density within the OFD zone in both Torlesse and non-Torlesse lithologies (Figure DR8), using the same approach as for Figures 3A and 3B of the main text. In both cases, the OFD zone had a generally higher landslide density suggesting that the influence of the OFD zone was independent of lithology.

> 2. We compared the distribution of lithologies within 2000 m of the fault to the distribution within the OFD zone (Table DR1). The proportion of lithology is very similar between the two zones suggesting that other factors likely explain the difference in the landslide distribution.

> 3. We examined the landslide density trends within each lithologic type separately (Figure DR9), We found that the very slight variations in lithologic proportion between the OFD zone and the area within 2000 m of the fault (Table DR1) do not explain a higher landslide density in the OFD zone. Quaternary sediments have the highest landslide density near the fault while Torlesse Greywacke has the lowest, yet, we see a slightly lower proportion of quaternary sediments (c. 4% less) and a slightly higher proportion of Torlesse (c. 2% more) in the OFD zone.
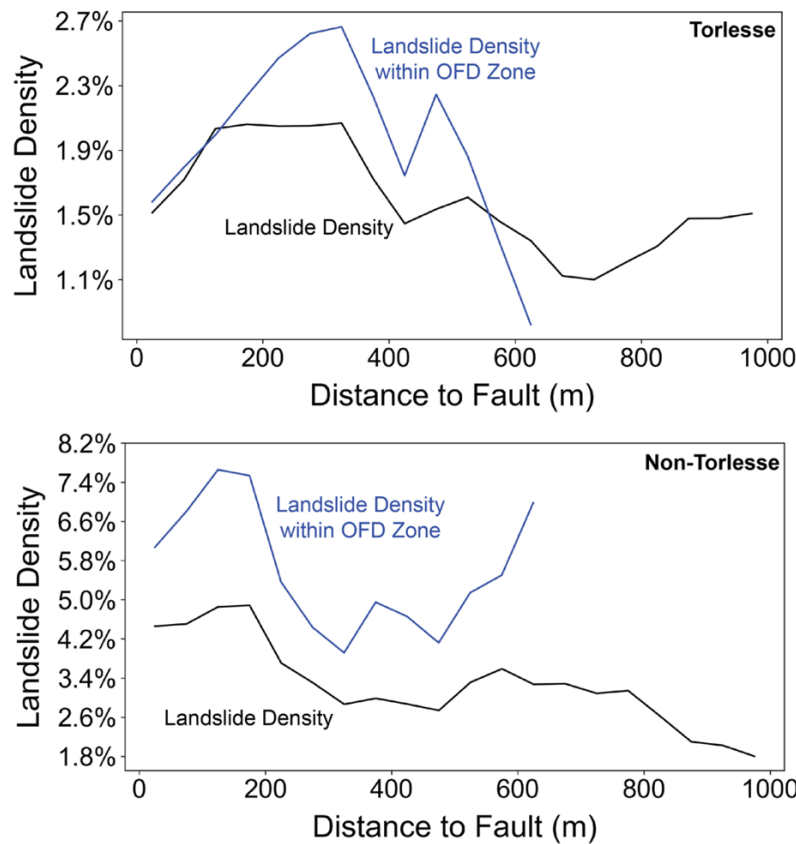
Figure DR8. Landslide Density to Fault Distance graph for Torlesse and Non-Torlesse lithologies. The black lines represent landslide density with general distance from fault while the blue lines represent landslide density with distance from the fault exclusively within the OFD zone. As a result of the variable width of the OFD zone, a smaller area is sampled by the OFD zone at greater fault distances. This may partially explain the spike in landslide density in non-Torlesse lithologies and the drop in landslide density in Torlesse lithology around 650 m from the fault.

Table DR1. Percent of area by GeolCode (Massey et al., 2020). GeolCode 1 is Quaternary sands, silts, and gravels, GeolCode 2 is Neogene limestones, sandstones, and siltstones, GeolCode 3 is Upper Cretaceous to Paleogene rocks including limestones, sandstones, siltstones, and minor volcanic rocks, GeolCode 4 is Lower Cretaceous Torlesse (Pahau terrane) basement rocks are predominantly sandstones and argillite, also known as greywacke. The OFD zone samples a relatively representative distribution of lithologies within 2000 m of the fault.

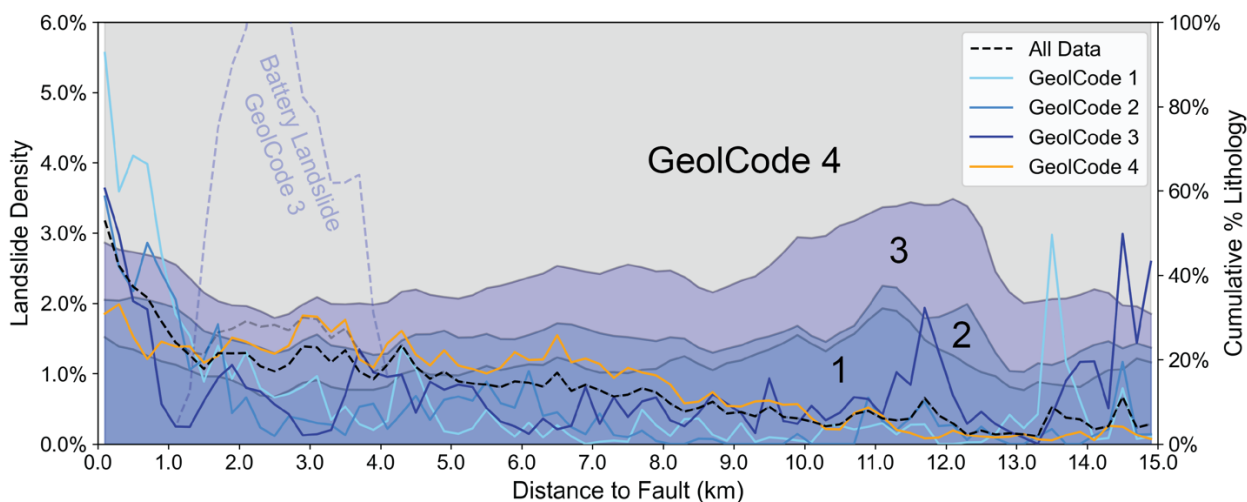| GeolCode	Geology Description	OFD Percent	2000 m Percent
1	*Quaternary Sediments*	15.68%	19.59%
2	*Neogene Sedimentary Rocks*	11.04%	11.53%
3	*Upper Cretaceous to Paleogene Sedimentary Rocks and Minor Volcanics*	12.37%	10.35%
4	*Lower Cretaceous Torlesse Greywacke (Pahau terrane)*	60.91%	58.54%

Figure DR9. Landslide Density to Fault Distance graph for GeolCodes 1 to 4 and the cumulative percent of each lithology with Distance to Fault. GeolCode 1 is Quaternary sands, silts, and gravels, GeolCode 2 is Neogene limestones, sandstones, and siltstones, GeolCode 3 is Upper Cretaceous to Paleogene rocks including limestones, sandstones, siltstones, and minor volcanic rocks, GeolCode 4 is Lower Cretaceous Torlesse (Pahau terrane) basement rocks are predominantly sandstones and argillite, also known as greywacke. Cumulative Percent of Lithology represents the percent of each lithology within 200 m bins.

The Battery Landslide

Our analysis of the landslide density with distance from the fault in individual lithologies (Figure DR9) revealed a large spike in landslide density in GeolCode 3 from c. 1 to 4 km from the fault. This spike, caused by the relict Battery landslide, correlates well with the spike we observe in landslide density from c. 1 to 3 km in non-Torlesse lithology (Figure 3D).

As discussed in the manuscript, we used a landslide dataset published by Massey et al. (2020) to derive our landslide density trends with distance from the fault. Our analysis includes all landslides in the database between 0 and 15 km of fault ruptures. This landslide database includes a few relict landslides that pre-date the 2016 Kaikōura earthquake but are known to have reactivated during the earthquake producing minor (< 1 m) displacements. The Battery landslide is the largest of these relict landslides and is, by far, the largest landslide source area in the database at c. 3 km^2 (more than 4 times as large as the next largest landslide). The Battery landslide occurs within GeolCode 3 between 1 and 3 km of the Humps fault but is uncharacteristic of failures in this material due to local site-specific changes in the geological materials.

If the source area of the Battery landslide is excluded from our analysis, we observe a generally consistent decay in landslide density with distance from the fault from c. 1 km to c. 13 km in all lithologies. Within c. 1 km of the fault we observe a much steeper decay in landslide density that may be partially explained by influences within the OFD zone. These findings correlate well with our general findings in Figure 3A and B.

Optical Image Correlation (OIC)

Zinke et al. (2019) also derived OFD zones for the 2016 Kaikōura event using perpendicular profiles of three-dimensional displacement fields generated from Optical Image Correlation (OIC) of pre- and post- event satellite imagery. On average, these OIC derived OFD zones are narrower than the zones we measured using the ICP displacement fields but generally show similar variations along fault strike (e.g. Figs. DR10, DR11). There are a number of explanations for these differences including the different spatial resolution of the datasets, different signal to noise ratios, and/or differences in the locations and interpretation of the fault perpendicular profiles. Further information on the ICP and OIC datasets themselves is available in Howell et al. (2020).

We performed an identical landslide density analysis on the faults and OFD zone derived by Zinke et al. (2019). The results of the general fault distance buffers matched well with our own landslide density analysis, however, the OFD zone derived from the OIC had a consistently lower landslide density than the synthetic buffers (e.g. 1.6% vs 3.1% at 200 m, Fig. DR12). This result is seemingly at odds with our analysis; however, several factors likely contribute to this discrepancy that we consider here.

First, our OFD Zone produced from ICP and interpolated between profiles is generally more continuous in landslide prone terrain than the OFD Zone produced from OIC by Zinke et al. (2019) (Figs. DR10 and DR11). Thus, the ICP OFD zone likely captures greater variation in the landslide density while the OIC derived data captures large areas, including the Emu Plains, that are not prone to landslides due to lack of topography (Fig. DR12). In areas with a more continuous zone of OFD produced from the OIC analysis, for instance about the Jordan Fault, landslide density trends align well with those of the ICP analysis and show a substantially higher landslide density within the OFD zone (Fig. DR13). Additionally, because noise was not manually removed from the OIC analysis, landslides themselves likely influence the selection of swath locations regionally. Where landslide densities were too high, measurements of the OFD zone were likely difficult to analyze due to a low signal to noise ratio. The ICP analysis, conducted at a lower resolution and including manual removal of identifiable noise, has an overall higher signal to noise ratio near landslides, making it possible to derive OFD widths despite the presence of slope failures.
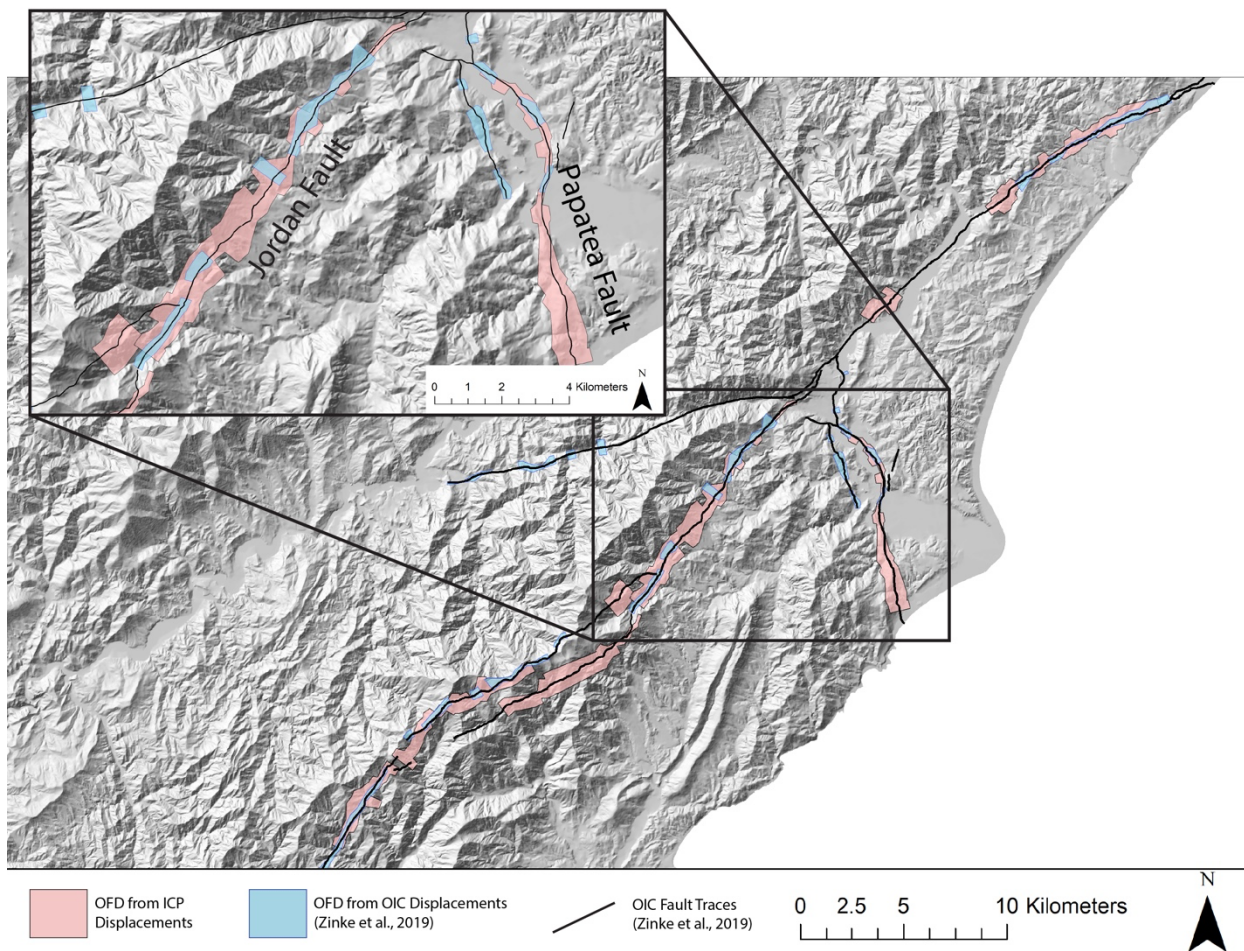
Figure DR10. Comparison of ICP and OIC (Zinke et al., 2019) derived OFD datasets. ICP derived OFD is generally wider and is interpolated over longer along strike fault segments. Examples include the southern Papatea Fault where landslide density is high.
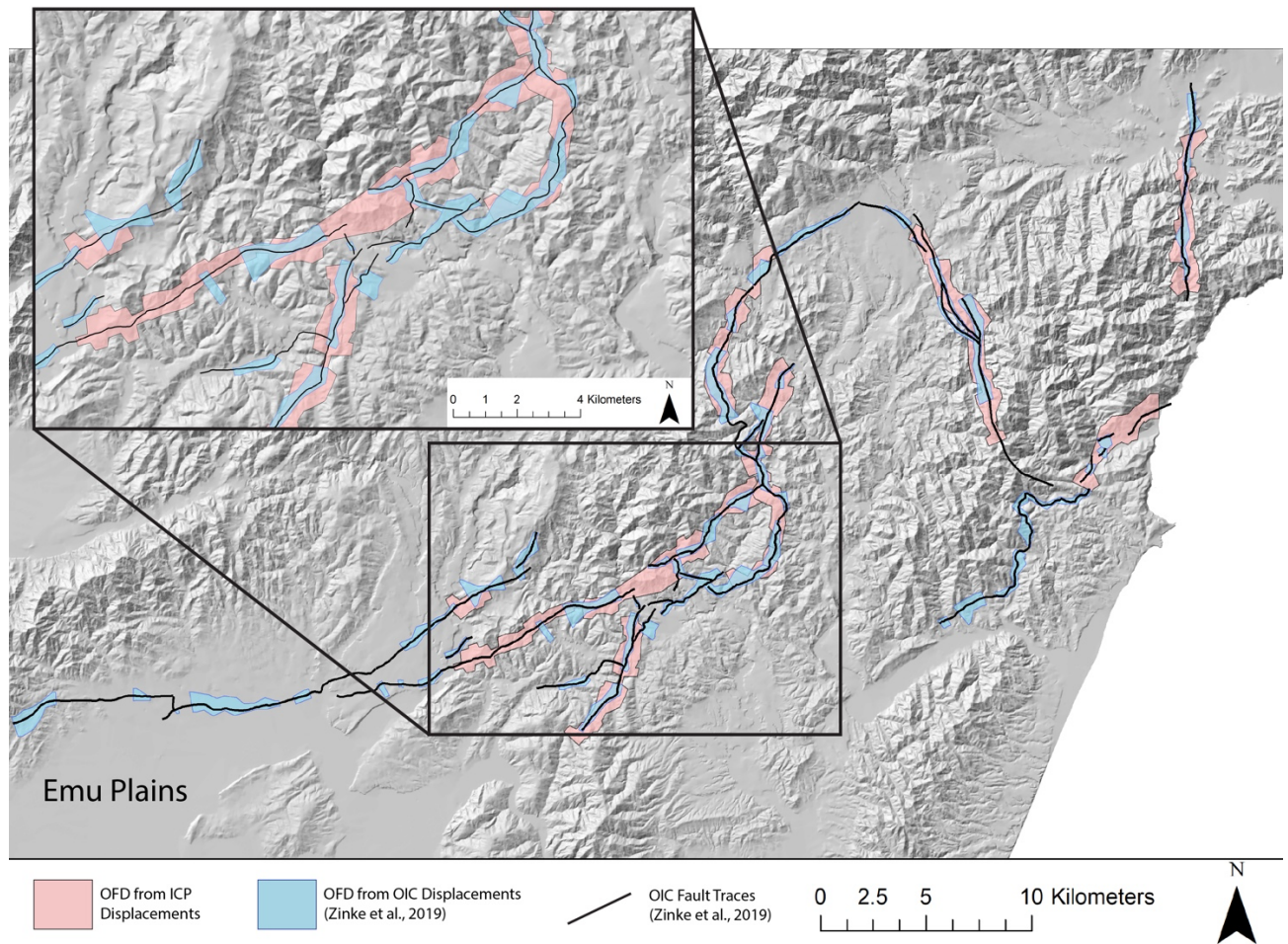
Figure DR11. Comparison of ICP and OIC (Zinke et al., 2019) derived OFD datasets. ICP derived OFD is generally interpolated over longer along strike fault segments in landslide prone terrain while OIC derived OFD is included in flat terrain not prone to landslides including the Emu Plains in the southwest corner of the main image.
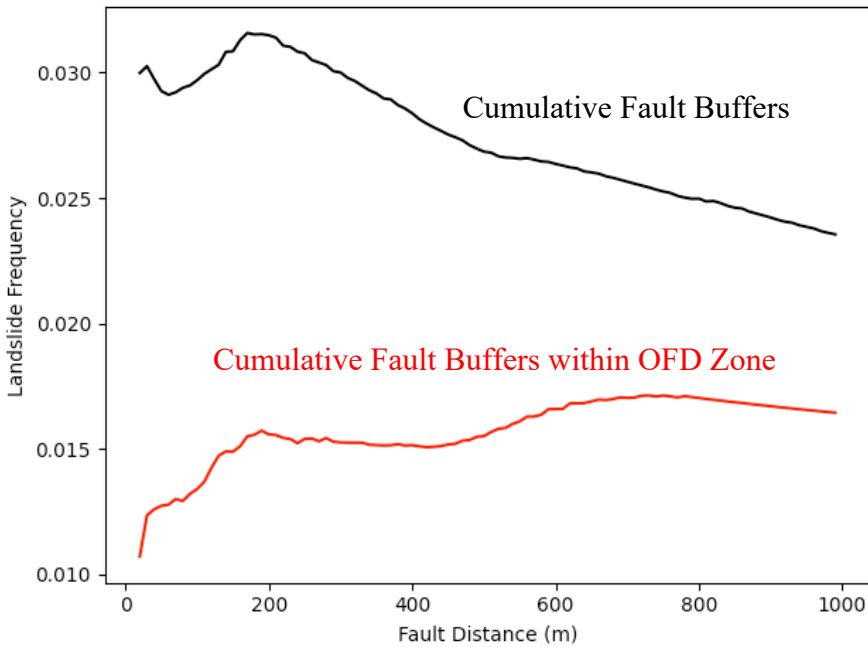
Figure DR12. Landslide Density to Fault Distance graph for all Kaikōura ruptures. Synthetic buffers from 10 to 1000 m about the fault (Black Line) produced from fault mapping by Zinke et al. (2019) and Landslide Density for OFD Zone (Red Line) produced by Zinke et al. (2019).
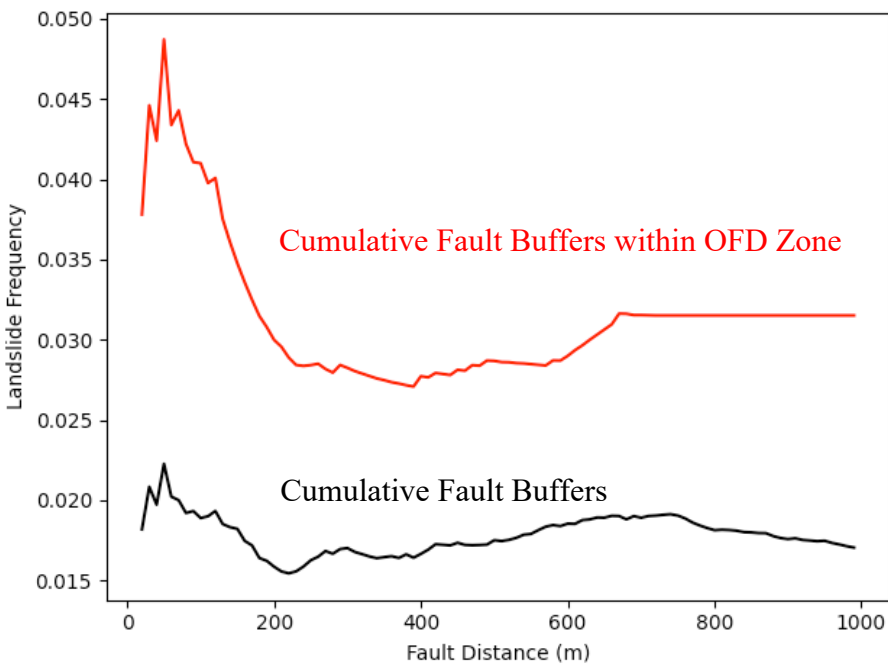

Figure DR13. Landslide Density to Fault Distance graph for the Jordan Fault. Synthetic buffers from 10 to 1000 m about the fault (Black Line) produced from fault mapping by Zinke et al. (2019) and Landslide Density for OFD Zone (Red Line) produced by Zinke et al. (2019).

Other Fault Datasets

In addition to our mapped traces, we determined the 'distance to fault' landslide density around several fault rupture datasets including the New Zealand Active Fault Database 250k Kaikōura Ruptures and those produced by Zinke et al. (2019). The longer length of these fault traces, often within flat terrain not susceptible to landslides, resulted in lower landslide density values. The smaller faults we traced using the ICP derived displacement fields represent a more conservative estimate of the landslide density with the 'distance to fault' parameter.

LANDSLIDE SOURCE AREA DENSITY BY FAULT

The landslide density trend we observe regionally within the OFD zone appears to be dominated by the highest slip faults in the MFS where most landslides were observed (Fig. DR14). In general, most individual faults show similar trends to the regional data set, however, in some cases, the distribution of landslides appears to be dominated by lithologic and topographic conditions that generally have more influence on coseismic landslide distributions than proximity to faulting and strong ground motion.

Extremely high topography around the Manakau, Upper Kowhai, and Snowflake Spur faults significantly influences the distribution of landslides (Fig. DR14). Variations from the regional trend observed on the Whites, Conway, and Stone Jug faults can largely be explained by the relatively few landslides in the vicinity of the faults (Fig. DR15). Discrepancies on the Humps East Fault are likely the result of interaction with the nearby Leader Fault (Fig. DR15). A low signal to noise ratio in the displacement field limited extensive measurements on some faults in the NCD including the Humps West and Hundalee faults. Collectively, these situations highlight that 'distance to fault' is one variable amongst many and local variations in, for instance topography and lithology, will modulate its importance.
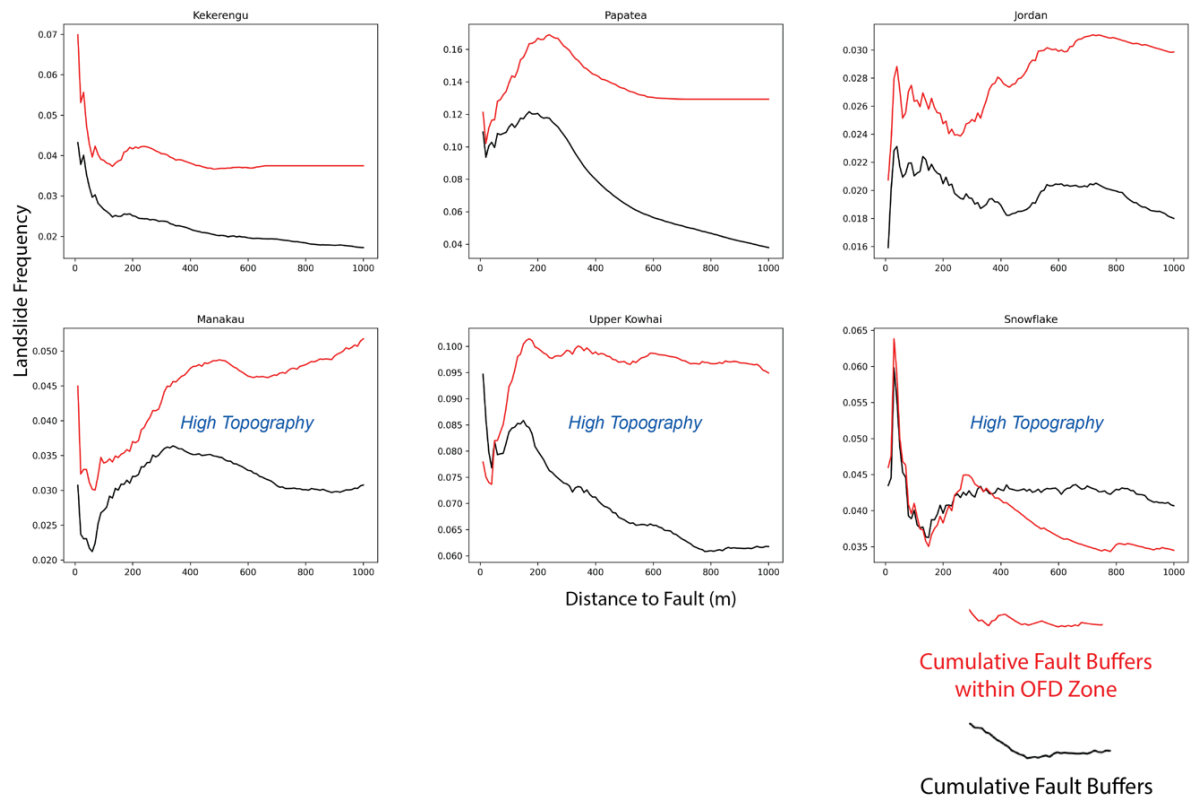
Figure DR14. Graph of landslide source area density compared to distance to fault for surface ruptured faults in the MFS.
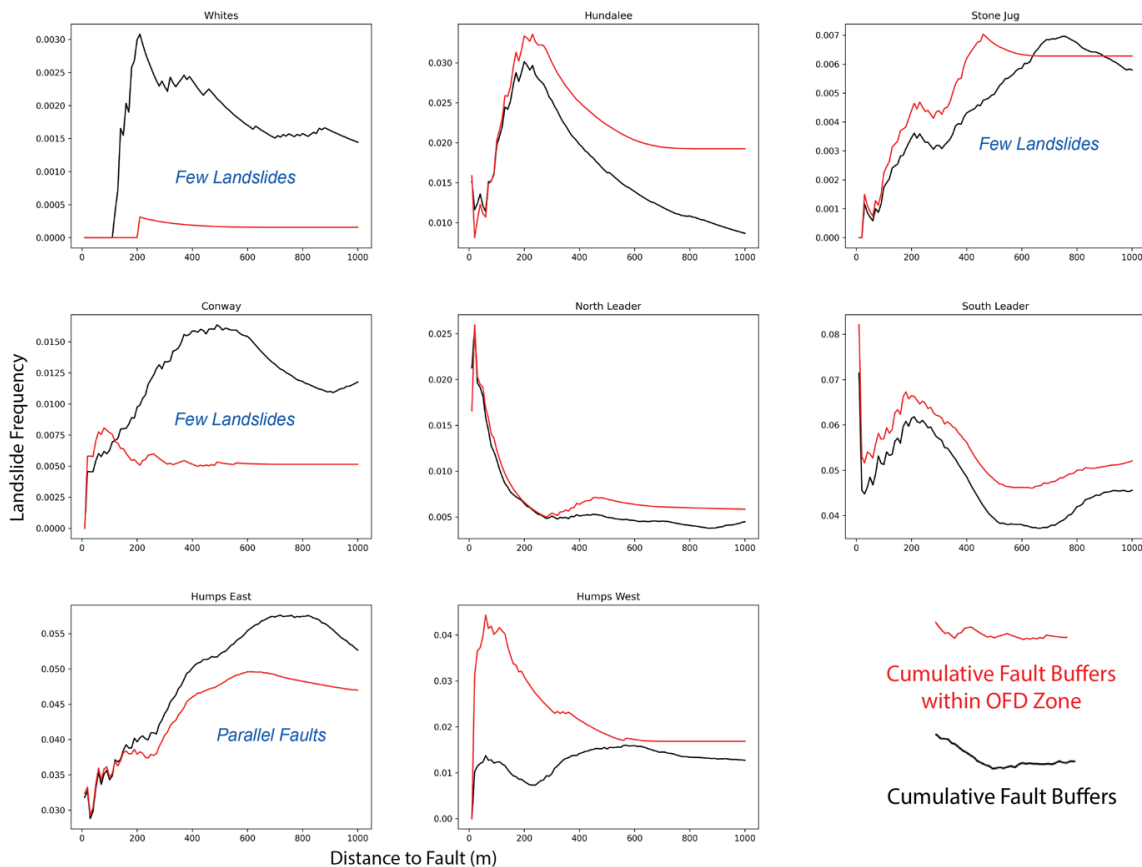
Figure DR15. Graph of landslide source area density compared to distance to fault for surface ruptured faults in the NCD.

References Cited

Bradley, B. A., Razafindrakoto, H. N. T., & Polak, V. (2017). Ground-motion observations from the 14 November 2016 M w 7.8 Kaikoura, New Zealand, earthquake and insights from broadband simulations. *Seismological Research Letters*, *88*(3), 740–756.

Holden, C., Kaneko, Y., D'Anastasio, E., Benites, R., Fry, B., & Hamling, I. J. (2017). The 2016 Kaikōura Earthquake Revealed by Kinematic Source Inversion and Seismic Wavefield Simulations: Slow Rupture Propagation on a Geometrically Complex Crustal Fault Network. *Geophysical Research Letters*, *44*(22), 11,320-11,328. https://doi.org/10.1002/2017GL075301

Howell, A., Nissen, E., Stahl, T., Clark, K., Kearse, J., Van Dissen, R., … Jones, K. (2020). Three-Dimensional Surface Displacements During the 2016 MW 7.8 Kaikōura Earthquake (New Zealand) From Photogrammetry-Derived Point Clouds. *Journal of Geophysical Research: Solid Earth*, *125*(1), 1–25. https://doi.org/10.1029/2019JB018739

Massey, C. I., Townsend, D. T., Lukovic, B., Morgenstern, R., Jones, K., Rosser, B., & de Vilder, S. (2020). Landslides triggered by the MW7.8 14 November 2016 Kaikōura earthquake: an update. *Landslides*, *17*(10), 2401–2408. https://doi.org/10.1007/DR10346-020-01439-x

Meunier, P., Hovius, N., & Haines, A. J. (2007). Regional patterns of earthquake-triggered landslides and their relation to ground motion. *Geophysical Research Letters*, *34*(20), 1–5. https://doi.org/10.1029/2007GL031337

Meunier, P., Uchida, T., and Hovius, N. (2013). Landslide patterns reveal the sources of large earthquakes. *Earth and Planetary Science Letters*, 363, 27–33. https://doi.org/10.1016/j.epsl.2012.12.018.

Rault, C., Robert, A., Marc, O., Hovius, N., and Meunier, P. (2019). Seismic and geologic controls on spatial clustering of landslides in three large earthquakes. *Earth Surface Dynamics*, 7, 829–839. 10.5194/esurf-7-829-2019.

Zinke, R., Hollingsworth, J., Dolan, J. F., & Van Dissen, R. (2019). Three-Dimensional Surface Deformation in the 2016 MW 7.8 Kaikōura, New Zealand, Earthquake From Optical Image Correlation: Implications for Strain Localization and Long-Term Evolution of the Pacific-Australian Plate Boundary. *Geochemistry, Geophysics, Geosystems*, *20*(3), 1609–1628. https://doi.org/10.1029/2018GC007951